Modelling Asymmetrical Facies Successions Using Pluri-Gaussian Simulations

Thomas Le Blévec, Olivier Dubrule, Cédric M. John, and Gary J. Hampson

Abstract An approach to model spatial asymmetrical relations between indicators is presented in a pluri-Gaussian framework. The underlying gaussian random functions are modelled using the linear model of co-regionalization, and a spatial shift is applied to them. Analytical relationships between the two underlying gaussian variograms and the indicator covariances are developed for a truncation rule with three facies and cut-off at 0. The application of this truncation rule demonstrates that the spatial shift on the underlying gaussian functions produces asymmetries in the modelled 1D facies sequences. For a general truncation rule, the indicator covariances can be computed numerically, and a sensitivity study shows that the spatial shift and the correlation coefficient between the gaussian functions provide flexibility to model the asymmetry between facies. Finally, a case study is presented of a Triassic vertical facies succession in the Latemar carbonate platform (Dolomites, Northern Italy) composed of shallowing-upward cycles. The model is flexible enough to capture the different transition probabilities between the environments of deposition and to generate realistic facies successions.

1 Introduction

Variogram-based indicator simulation aims to distribute facies in space using first- and second-order spatial statistics as a constraint. It is widely used for modelling heterogeneous subsurface rock volumes such as hydrocarbon reservoirs and groundwater aquifers, in which data are usually sparse and deterministic methods are not appropriate. In standard oil industry practice, the facies represent regions of the reservoir where petrophysical properties such as porosity and permeability can be assumed to have statistically homogeneous distributions. Therefore, the spatial distribution of facies has a great impact on the reservoir model predictions.

T. Le Blévec (✉) • O. Dubrule • C.M. John • G.J. Hampson
Imperial College, Royal School of Mines, Prince Consort Road, London SW7 2BP, UK
e-mail: t.le-blevec15@imperial.ac.uk; o.dubrule@imperial.ac.uk; cedric.john@imperial.ac.uk; g.j.hampson@imperial.ac.uk

While it is easy to constrain the models with the proportion and autocovariance of each facies (Alabert 1989; Armstrong et al. 2011), it is more complex to model the cross-indicator covariances between facies. For instance, SIS (sequence indicator simulation) by modelling every facies independently (Alabert 1989) does not reproduce cross-covariances between different facies, possibly resulting in non-realistic geological models.

With the aim of modelling spatial relationships between different facies, Carle and Fogg (1996) constrain cross-covariances using the parameters of a continuous-time Markov chain. An important outcome of their method is the possibility to model spatial asymmetry between the indicator variables. The probability of facies A to be on top of facies B can be different from that of facies A being under B. Such asymmetrical vertical stacking patterns of facies are common in the stratigraphic record as sedimentological processes tend to create and preserve shallowing-upward facies successions which are asymmetric (Burgess et al. 2001; Grotzinger 1986; Strasser 1988; Tucker 1985). However, the model used by Carle and Fogg (1996) is memoryless and so prevents from using a hole-effect covariance and reproducing cyclicity, which is another common feature of vertical facies successions (Burgess et al. 2001; Fischer 1964; Goldhammer et al. 1990; Grotzinger 1986; Masetti et al. 1991). Another approach uses non-parametric indicator variograms for bivariate probabilities to simulate facies with asymmetrical patterns (Allard et al. 2011; D'Or et al. 2008). The approach presented in the current paper aims to use parametric auto- and cross-covariance models that are "realizable", that is associated with valid random set models (Chilès and Delfiner 2012).

Pluri-Gaussian simulations (PGS) can handle facies interactions thanks to the use of underlying continuous gaussian variables and truncation rules defining facies ordering and geometries (Armstrong et al. 2011). Moreover, by construction, the PGS formalism leads to a general cross-covariance model between facies that is realizable (Chilès and Delfiner 2012). Developing a flexible multivariate gaussian framework allows to increase the range of facies patterns. For instance, the original linear model of co-regionalization (Wackernagel 2013), applied to the underlying gaussian functions, provides flexibility in the resulting facies thicknesses and distributions. However, the cross-correlations between the underlying gaussian functions are symmetrical and so are the facies relations.

To overcome this limitation, some authors have proposed to use spatial shifts to transform the cross-covariances between gaussian functions (Apanasovich and Genton 2010; Li and Zhang 2011; Oliver 2003). Armstrong et al. (2011) proposed to use a similar approach when defining the linear model of co-regionalization of the underlying gaussian variables. Although it is natural to expect that an asymmetrical cross-correlation between the gaussian functions should lead to asymmetrical relations between facies, this approach has not yet, to our knowledge, been fully developed and tested. Moreover, the relation between the spatial shift, the correlation and the facies asymmetry has not been studied explicitly.

In this article, we expand on the previous work described above to demonstrate that a spatial shift applied to the underlying gaussian functions can be used to create asymmetries in the vertical stacking of facies. The sensitivity of vertical facies

stacking patterns to selected parameters is then investigated. Synthetic examples are produced, and the usefulness of this method is demonstrated by modelling a real facies succession from the Triassic Latemar carbonate platform (Dolomites, Northern Italy).

2 Methodology

In this section, we explain the basic principles of the pluri-Gaussian simulation (PGS) methodology and its relation to indicator functions. We then describe the shifted PGS model.

2.1 Context and Notations

We focus here on a simple example with three facies. The truncation rule that defines the contacts between facies and their proportion, relative to their area, can be drawn as follows (Fig. 1):

If I_1, I_2 and I_3 are the indicators of the three facies, the truncation rule defines them as follows for every location x on a vertical section:

$$I_1(x) = \begin{cases} 1, \ Z_1(x) < t_1 \\ 0, \ else \end{cases} \tag{1}$$

$$I_2(x) = \begin{cases} 1, \ Z_1(x) > t_1, Z_2(x) > t_2 \\ 0, \ else \end{cases} \tag{2}$$

$$I_3(x) = \begin{cases} 1, \ Z_1(x) > t_1, Z_2(x) < t_2 \\ 0, \ else \end{cases} \tag{3}$$

When the indicator of a facies equals 1, the corresponding facies is present at the location x. The marginal gaussian cumulative function G applied to each gaussian function Z_1 and Z_2 allows to have a truncation rule on which the area of a facies equals its proportion. However, if there is a correlation between the two functions, it affects the proportion as the points tend to be located along the transformation of the correlation line ρ (Fig. 1) which is plotted in the axes $(G(Z_1),G(Z_2))$ and thus has for equation

$$Y = G\left[\rho*G^{-1}[X]\right] \tag{4}$$

In the example of Fig. 1, a positive correlation increases the proportion of facies 2 over facies 3 as shown by the larger number of points generated in the domain of facies 2. With a negative correlation, it would be the opposite. A uniform truncation
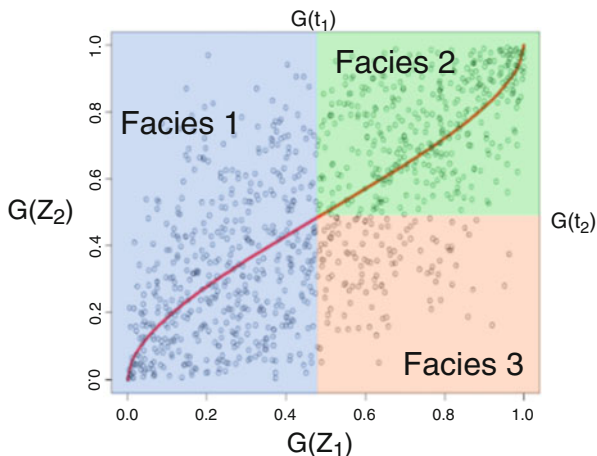
Fig. 1 Truncation rule defining three facies with two gaussian random functions Z_1 and Z_2. t_1 and t_2 are the truncations associated with each gaussian functions and G is the gaussian cumulative function. The *red curve* is defined by Eq. 4, with the correlation $\rho = 0.7$. One thousand random generations with a correlation $\rho = 0.7$ are performed thanks to the R package MASS (Venables and Ripley 2002) and displayed

rule could be obtained by applying the bi-normal gaussian cumulative function with correlation ρ on Z_1 and Z_2, but its analytical expression is not known.

The truncation rule does not contain spatial information and so does not control asymmetries. As the aim of this study is to model asymmetrical relations, the transition probability from one facies i to another j should be different in opposite directions h and $-h$:

$$t_{ij}(h) = \frac{P\left[I_i(x) = 1, I_j(x+h) = 1\right]}{P[I_i(x) = 1]} \neq t_{ij}(-h) \tag{5}$$

Under the stationary hypothesis, the transition probability is independent of location. This transition probability results from the gaussian function parameters: correlation ρ, thresholds t_1 and t_2, gaussian correlation models $\rho z_1(h)$ and $\rho z_2(h)$ and the cross-correlation $\rho z_1 z_2(h)$ that can be asymmetric.

2.2 *Relation Between the Indicators and Gaussian Functions*

Understanding the link between the facies transition probabilities and the parameters of the underlying bi-gaussian function would help in inferring a pluri-Gaussian model resulting in the correct asymmetrical transition probabilities. Armstrong et al. (2011) show that the covariance of the facies indicator can be expressed as a multivariable integral of the underlying bi-gaussian density. For instance, the non-centred cross-covariance, between facies 2 and 3, $C_{23}(h)$, is defined as

$$C_{23}(h) = E[I_2(x)\,I_3(x+h)] = P[I_2(x) = 1, I_3(x+h) = 1] \tag{6}$$

According to Eqs. 1, 2 and 3, we have

$$C_{23}(h) = P[Z_1(x) > t_1, Z_2(x) > t_2, Z_1(x+h) > t_1, Z_2(x+h) < t_2] \tag{7}$$

This is the joint probability of four gaussian events with their dependence described by the correlation matrix:

$$\sum(h) = \begin{pmatrix} 1 & \rho & \rho_{Z_1}(h) & \rho_{Z_1 Z_2}(h) \\ \rho & 1 & \rho_{Z_1 Z_2}(-h) & \rho_{Z_2}(h) \\ \rho_{Z_1}(h) & \rho_{Z_1 Z_2}(-h) & 1 & \rho \\ \rho_{Z_1 Z_2}(h) & \rho_{Z_2}(h) & \rho & 1 \end{pmatrix} \tag{8}$$

$C_{23}(h)$ can then be expressed as an integral of the quadri-variate gaussian density $g_{\Sigma(h)}(u,v,w,z)$ with the covariance matrix previously described:

$$C_{23}(h) = \int_{t_1}^{\infty} \int_{t_2}^{\infty} \int_{t_1}^{\infty} \int_{-\infty}^{t_2} g_{\sum(h)}(u,v,w,z)\,du\,\,dv\,\,dw\,\,dz \tag{9}$$

As we work with three facies (Fig. 1), the covariance between facies 1 and facies 2 is expressed by a triple integral, while a double integral defines the autocovariance of facies 1.

2.3   The Spatial Shift Applied to the Linear Model of Co-regionalization

The linear model of co-regionalization presented by Wackernagel (2013) is a flexible model for p-multivariate simulations and is chosen in this article. We also incorporate a shift on the covariance matrix C as proposed by Li and Zhang (2011). Armstrong et al. (2011) propose a way to simulate such a multivariate field from two independent gaussian functions Y_1 and Y_2 with covariances $\rho_{Y_1}(h)$ and $\rho_{Y_2}(h)$:

$$\begin{cases} Z_1(x) = Y_1(x) \\ Z_2(x) = \dfrac{\rho}{\rho_{Y_1}(a)} Y_1(x+a) + \sqrt{1 - \dfrac{\rho^2}{\rho_{Y_1}(a)^2}}\, Y_2(x) \end{cases} \tag{10}$$

The spatial shift, a, is the distance at which the correlation between the two gaussian functions Z_1 and Z_2 is maximal, and ρ is the correlation between the two simulated gaussian functions Z_1 and Z_2 at the same location. We can directly deduce from the square root term in Eq. 10 the condition of validity of the model:

$$-\rho_{Y_1}(a) < \rho < \rho_{Y_1}(a) \tag{11}$$

This condition originally results from the fact that the variance of the gaussian functions Z_1 and Z_2 is one. It is now possible to relate the covariances ρ_{Z_1} and ρ_{Z_2} of the gaussian fields Z_1 and Z_2 to the covariances of Y_1 and Y_2:

$$\begin{cases} \rho_{Z_1}(h) = \rho_{Y_1}(h) \\ \rho_{Z_2}(h) = \dfrac{\rho^2}{\rho_{Y_1}(a)^2}\rho_{Y_1}(h) + \left[1 - \dfrac{\rho^2}{\rho_{Y_1}(a)^2}\right]\rho_{Y_2}(h) \end{cases} \tag{12}$$

and the cross-correlations between Z_1 and Z_2, which are asymmetric:

$$\begin{cases} \rho_{Z_1Z_2}(h,a) = \dfrac{\rho\rho_{Z_1}(|h+a|)}{\rho_{Z_1}(a)} \\ \rho_{Z_1Z_2}(-h,a) = \dfrac{\rho\rho_Z(|h-a|)}{\rho_{Z_1}(a)} \end{cases} \tag{13}$$

It is interesting to see that

$$\rho_{Z_1Z_2}(-h,-a) = \rho_{Z_1Z_2}(h,a) \tag{14}$$

The different parameters of the model are summarized in Table 1.

Table 1 Symbols of the different parameters of the shifted pluri-Gaussian model

Signification	Parameter
First gaussian field	Z_1
Second delayed gaussian field	Z_2
Upward transition probability from facies i to facies j as a function of distance h	$t_{ij}(h)$
Proportion of facies i	P_i
Covariance function of Z_1	$\rho_{z_1}(h)$
Covariance function of Z_2	$\rho_{z_2}(h)$
Correlation coefficient between Z_1 and Z_2	ρ
Cross-correlation between Z_1 and Z_2 at distance h	$\rho_{z_1z_2}(h)$
Shift in the cross-correlation between Z_1 and Z_2	a
Range of the first gaussian function with a gaussian variogram, practical range $a_1\sqrt{3}$	a_1
Range of the second gaussian function with a gaussian variogram, practical range $a_2\sqrt{3}$	a_2

3 Results

In this section, we study the indicator transiograms derived from the shifted linear model of co-regionalization applied with PGS and with the truncation rule in Fig. 1. We first express the analytical expressions for a special case and then develop a sensitivity study in the general case thanks to numerical gaussian integrations. Gaussian variograms for the gaussian functions are used in order to have a linear behaviour at the origin on the indicator transiograms.

3.1 Analytical Study of the Asymmetry

We focus here on the special case where $t_1 = t_2 = 0$ as some analytical expressions can be found between the pluri-Gaussian and the transition probabilities.

3.1.1 Behaviour of the Asymmetrical Transition Probability

With the truncation rule used in Fig. 1, the transition probability between facies 1 and 2 can be written as a triple integral. Its analytical expression, developed in the appendix (Eqs. 25 and 26), is the following:

$$t_{12}(h) = -\frac{1}{4} + \frac{1}{2\pi}\left[\arccos\left(\frac{\rho\rho_{Z_1}(|h+a|)}{\rho_{Z_1}(a)}\right) + \arccos\left(\rho_{Z_1}(h)\right) + \arcsin(\rho)\right] \quad (15)$$

Therefore, the shift a and the correlation ρ must be non-zero to bring asymmetry (Fig. 2). We can also deduce the relation:

$$t_{12}(-h, -a) = t_{12}(h, a) \quad (16)$$

which means that changing the sign of the shift allows the asymmetry between the two facies to be switched.

We can see that if the correlation and shift are positive, and the transition probability tends towards a facies with low proportions, the curve has a very high concavity with a maximum before the range (Fig. 2, right). If the correlation is negative and the transition probability tends towards a facies with high proportion, the curve has an inflexion point (Fig. 2, left). In the opposite direction, the behaviour is always different, highlighting the asymmetry. If there is no shift, there is no asymmetry (Fig. 2).
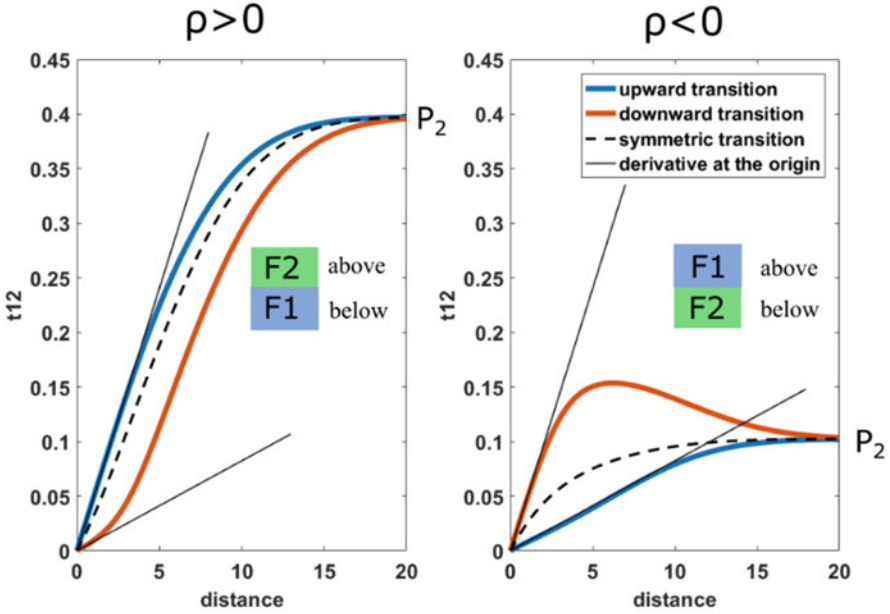
Fig. 2 Influence of a positive shift on the transition probabilities from facies 1 to facies 2 with different values of the proportion P_2 of facies 2. The coefficient ρ is either 0.8 or -0.8. The gaussian function has a gaussian variogram with range 8 (practical range = 13.85) and the shift is 3. The upward and downward transitions are deduced from Eq. 15, such as the *dotted line* obtained with a shift equal to 0, and the *black* tangents are obtained from Eqs. 17 to 18

3.1.2 Asymmetry in Facies Contacts

The frequency of contacts between two given facies can be derived from the derivative of the cross-transition probability at the origin, which is the rate of transition from one facies to the other per unit length. We can express the rate of transition upward $T_{12}{}^+$ and downward $T_{12}{}^-$ in the case of a gaussian variogram by differentiating Eq. 15:

$$T_{12}^{+}(a,\rho,a_1) = \lim_{h\to 0} t_{12}{}'(h) = \frac{1}{2\pi}\left[\frac{\sqrt{2}}{a_1} + a\frac{2\rho}{a_1^2\sqrt{1-\rho^2}}\right] \tag{17}$$

$$T_{12}^{-}(a,\rho,a_1) = \lim_{h\to 0} t_{12}{}'(-h) = \frac{1}{2\pi}\left[\frac{\sqrt{2}}{a_1} - a\frac{2\rho}{a_1^2\sqrt{1-\rho^2}}\right] \tag{18}$$

From these equations, it is clear that if the correlation ρ and the shift a are positive, the probability of having facies 2 on top of facies 1 is higher than of having facies 1 on top of facies 2. It can be interesting to see for which shift the transition rate is maximal; let's take

$$a_{\lim} = a_1 \frac{\sqrt{2(1 - \rho^2)}}{2\rho} \qquad (19)$$

In that case, we have

$$\begin{cases} T_{12}^+(a_{\lim}, \rho, r_1) = \dfrac{\sqrt{2}}{a_1 \pi} \\ T_{12}^-(a_{\lim}, \rho, r_1) = 0 \end{cases} \qquad (20)$$

With this shift, facies 1 cannot make a transition to facies 2 going downwards as the transition rate is 0. For the upward transition, it can be noticed that the expression of the transition rate is the inverse of the mean length of facies 1 (Lantuéjoul 2002). This implies that the upward transition rate from facies 1 to facies 3 is zero with the closing relations of the transition rate matrix Q:

$$Q = \begin{pmatrix} -1/L_1 & 1/L_1 & 0 \\ 0 & -1/L_2 & 1/L_2 \\ -1/L_3 & 0 & -1/L_3 \end{pmatrix} \qquad (21)$$

with L_i as the mean lengths of the different facies. Therefore, this shift gives the maximum of asymmetry and allows to build perfect geologic asymmetrical sequences. However, the shift is also bounded by Eq. 11, and consequently Eqs. 19, 20 and 21 are not possible. As the transition rates increase linearly with the shift, the maximum of asymmetry is obtained for the higher shift which is the following according to Eq. 11:

$$a_{\max} = a_1 \sqrt{-\log(\rho)} \qquad (22)$$

It can be noted that the expressions of $a_{\lim}$ and $a_{\max}$ converge to each other when ρ tends to one. Thus, for a correlation that tends to one, $a_{\max}$ gives upward and downward transition rates that tend, respectively, to $1/L_i$ and 0, allowing to create perfect asymmetrical sequences (Eq. 21). This limit case can also be obtained by simulating only one gaussian function and use the shifted equivalent as the second gaussian function.

The expressions of the multi-gaussian integrals have allowed asymmetries for a truncation rule with cut-off at 0 to be analytically expressed. Lantuéjoul (2002) gives a solution for a general truncation rule when the correlation tends to 1. This might allow development of more general expressions with thresholds.

3.2 Sensitivity Analysis for a General Truncation Rule

The gaussian integral cannot be computed analytically in the general case with cut-offs different from 0. However, it can be computed numerically (Genz 1992)
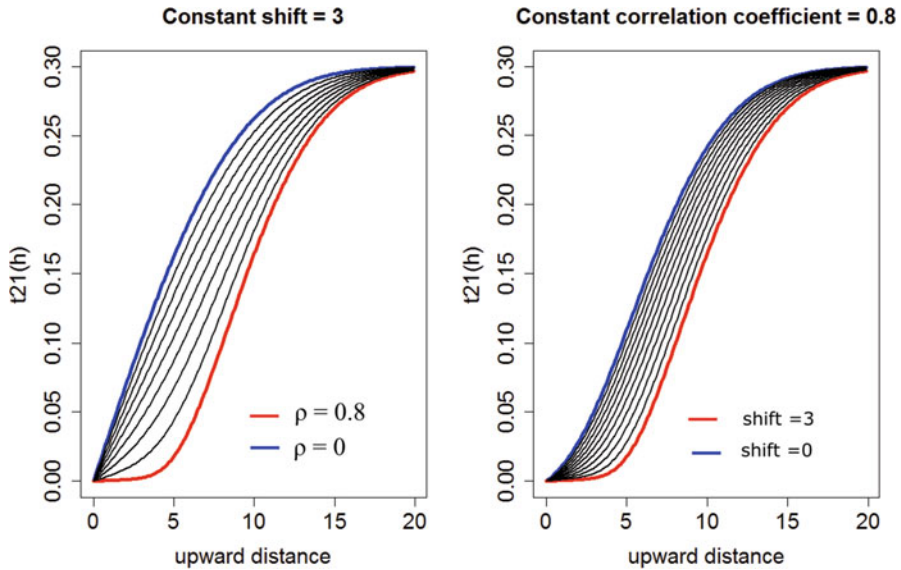
Fig. 3 Comparison of the impact of the correlation and the shift on the transition probability from facies 2 to facies 1 upwards. The step for the *black curves* is 0.1 for the correlation (*left*) and 0.3 for the shift step (*right*). The range of the first gaussian variogram is 8, the proportion of facies 1 is 0.3 and facies 2 is 0.4

using a code available on R (Genz et al. 2009; Renard et al. 2015). Consequently, we have access to all the transition probabilities, and the correlation ρ can be changed while keeping the proportions constant which is not possible analytically.

This is carried out by minimizing an objective function quantifying the difference between the targeted and simulated proportions computed with the gaussian numerical integral (Genz 1992). It can also be done with a maximum likelihood estimation of the target proportions by generating random correlated gaussian values. Understanding the impacts of the correlation and the shift at constant proportions is important for manually fitting transition probabilities (Fig. 3).

We can see in Fig. 3 that both the correlation and the shift have an impact on the tangent at the origin which provides a flexibility to match the asymmetry between facies contacts. The asymmetrical limit behaviour a_{lim} (Eq. 19) seems to have been reached with $\rho = 0.8$ and $a = 3$ as the transition rate is close to 0 for these values. The two parameters also affect differently the curvature of the transition probability increasing the flexibility of the method.

4 Case Study

This section presents a case study for illustrating the method described earlier with three facies and the truncation rule of Fig. 1. The geostatistical package RGeostats is used for the simulation (Renard et al. 2015). The transiograms are studied for two facies as the relation with the third can be automatically deduced from them.

4.1 The Latemar Data Set

Carbonate outcrops usually show significant vertical asymmetries in their facies distribution, in part explained by a gradual lateral shift in environments of depositions during sea-level highstands, followed by nondeposition during sea-level lowstands and the subsequent transgression (Catuneanu et al. 2011). For instance, the intertidal environment tends to be on top of the subtidal environment in shallowing-upward sequences (Sena and John 2013). The Latemar massif in the Dolomites of Northern Italy shows well-documented examples of asymmetrical vertical facies sequences in a carbonate platform. As reported by Egenhoff et al. (1999), a typical asymmetrical, upward-shallowing succession is bounded by a supratidal exposure surface at its top, which tends to cap intertidal-to-shallow-subtidal grainstones that overlie subtidal wackestones (Fig. 4).

4.2 Constraining the Transition Probabilities

The transition probabilities of Fig. 5 were derived from the data shown in Fig. 4. They can be fitted with the shifted linear model of co-regionalization manually through a trial-and-error process, by maximum likelihood estimation or by minimizing an objective function. In a more general context, a manual procedure is preferred as transiogram modelling is a step where geological conceptual knowledge can be incorporated. Therefore, we choose to fit manually the transition probabilities of Fig. 5.

As seen in Fig. 5, the model fitted by trial and error honours the tangent at the origin of the transition probabilities. This means that the transition rates are well constrained. Moreover, a possible hole-effect is observed in the experimental transition probabilities due to a low variance in the facies thicknesses. This effect cannot be modelled with the current model, but a hole-effect variogram on the gaussian function should be able to model it (Dubrule 2016).
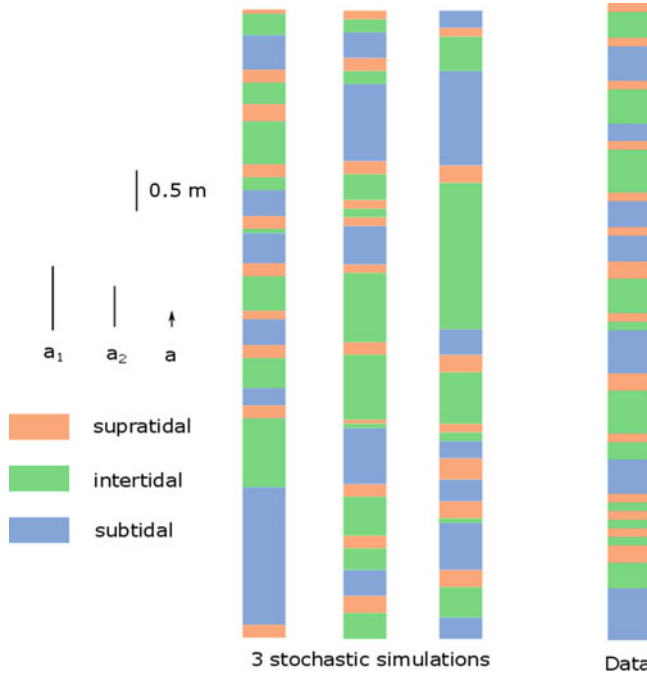
Fig. 4 Comparison between the vertical section of the Latemar section reported by Egenhoff et al. (1999) and simulations with asymmetrical pluri-Gaussian simulations. The parameters for the simulation are the same as described in Fig. 5
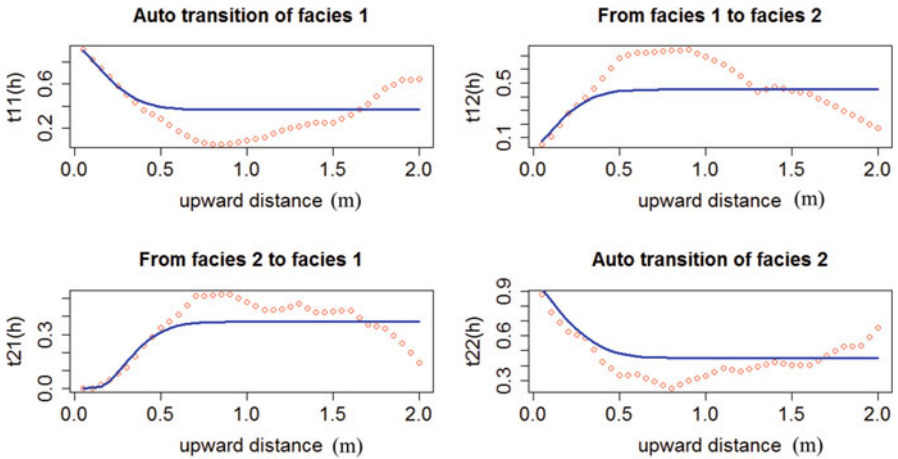

Fig. 5 Match between experimental transition probabilities (*red*) observed in Fig. 4 and the model (*blue*). Facies 1 is subtidal and facies 2 intertidal. The parameters used for the model are 0.9 for the range of the first gaussian, 0.52 for the range of the second gaussian, 0.13 for the shift and 0.8 for the correlation
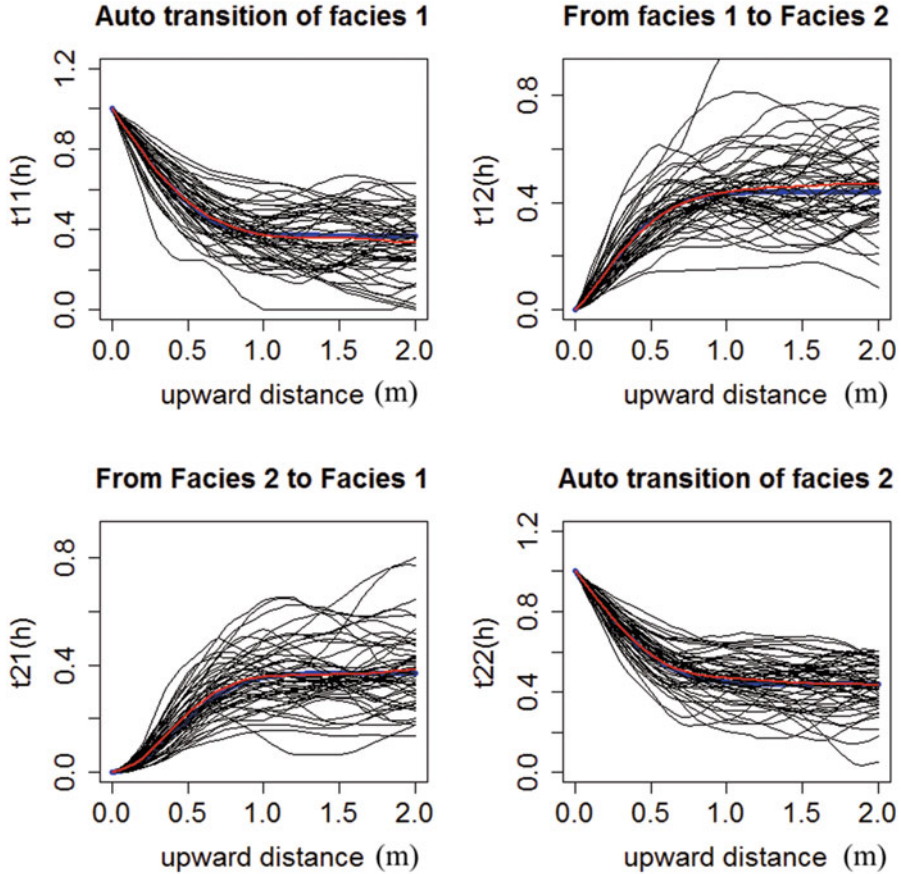
Fig. 6 Comparison between transition probabilities model (*blue*) and simulated (*grey*) and mean of the simulated (*red*) on 50 simulations of the Latemar section presented in Fig. 4. Facies 1 is subtidal, and facies 2 is intertidal

4.3 Facies Asymmetrical Simulation with Pluri-Gaussian Model

We build two gaussian fields, and then we apply the transformations described in Eq. 10 on three simulations (see Fig. 4). The asymmetry is still preserved in the simulations, with supratidal facies always on top of the intertidal facies and the intertidal facies on top of the subtidal facies. However, the limit shift a_{lim} (Eq. 19) has not been reached as the probability of having subtidal on top of supratidal is not 1, which is also observed on the data. To go further in the simulation analysis, the experimental transiograms are computed on 50 simulated sections and compared to the model variogram (Fig. 6).

This Monte Carlo study shows that the simulated transition probabilities seem to match the model well at the origin and for other distances as the mean transiogram of the simulations matches with the transiogram model (Fig. 6).

5   Discussion and Conclusion

This study has shown that the shifted linear model of co-regionalization seems well-suited to model facies transitions asymmetries using PGS. For the case of modelling three facies, the first two gaussian variograms allow to define facies mean thicknesses, while the shift and the correlation determine the asymmetrical patterns. Therefore, every transition rate of the transiogram matrix can be inferred independently making the method very flexible. Moreover, we saw analytically and numerically that the maximum rate of transitions could be reached asymptotically, which allows to build perfect asymmetrical sequences.

More precisely, the gaussian integral allows to fix the transition rates as with a Markov process (Carle and Fogg 1996). However, if the number of facies is increased, it would be more difficult to respect the different asymmetries, and manual fitting of the different transition probabilities would be more complex. Automatic procedures such as maximum likelihood estimations might address that issue.

The advantage of PGS over continuous-time Markov chains is that it provides a framework in which the resulting indicator variograms are automatically valid but also quite flexible. Beyond just transition rates, the parametrical covariances can lead to linear or fractal behaviour of the indicator variogram at the origin (Chilès and Delfiner 2012; Dubrule 2016). Other models than the linear model of co-regionalization would allow to select different behaviours for every facies. For instance, the multivariate Matern model would allow cross-transition probabilities to have different smoothness parameters for every facies (Gneiting et al. 2012), and the spatial shift could be applied to it (Li and Zhang 2011) which would also result in facies asymmetries. This is currently investigated by the authors.

Appendix: Analytical Expression of the Triple Gaussian Integral

In a similar fashion as Kendall et al. (1994), we consider three correlated gaussian variates being in their respective intervals as a set of three dependent events. With the truncation rule displayed in Fig. 1 and thresholds that equal 0, facies 1 at

location x and facies 2 at location $x+h$ correspond to one variate being negative and two positive. The indicator covariance $C_{12}(h)$ quantifies the probability of the intersection of these three events. The correlation matrix between the three gaussian variates is the following:

$$\sum(h) = \begin{pmatrix} 1 & \rho_{Z_1}(h) & \dfrac{\rho\rho_{Z_1}(|h+a|)}{\rho_{Z_1}(a)} \\ \rho_{Z_1}(h) & 1 & \rho \\ \dfrac{\rho\rho_{Z_1}(|h+a|)}{\rho_{Z_1}(a)} & \rho & 1 \end{pmatrix} \tag{23}$$

The probability can be written as a triple integral of the corresponding gaussian density $g_{\Sigma(h)}(u,v,w)$:

$$C_{12}(h) = \int_{-\infty}^{0} \int_{0}^{+\infty} \int_{0}^{+\infty} g_{\Sigma(h)}(u,v,w)\,dudvdw \tag{24}$$

Thanks to the gaussian integral symmetry property, the probability of intersection of the events is the complementary of the probability of their union (Kendall et al. 1994). Therefore, by definition of the union, the intersection of the three events can be expressed as a sum of the corresponding single and pair events and so the triple integral as a sum of the single integrals that equal to 0.5 and double integrals with their respective correlation coefficient:

$C_{12}(h)$

$$= \frac{1}{2} \left(1 - 3*0.5 + \int_{-\infty}^{0} \int_{0}^{+\infty} g_{\rho_{Z_1}(h)}(u,v)\,dudv + \int_{-\infty}^{0} \int_{0}^{+\infty} g_{\frac{\rho\rho_{Z_1}(|h+a|)}{\rho_{Z_1}(a)}}(u,v)\,dudv \right.$$

$$\left. + \int_{0}^{+\infty} \int_{0}^{+\infty} g_{\rho}(u,v)\,dudv \right) \tag{25}$$

Sheppard (1899) gives then the solution of the double integral that allows to obtain the final expression of the transition probability between facies 1 and 2 (Eq. 15):

$$\int_{0}^{+\infty} \int_{0}^{+\infty} g_{\rho}(u,v)\,dudv = \frac{1}{2} - \int_{0}^{+\infty} \int_{0}^{+\infty} g_{\rho}(u,v)\,dudv = \frac{1}{4} + \frac{1}{2\pi}\arcsin(\rho) \tag{26}$$

Bibliography

Alabert F (1989) Non-Gaussian data expansion in the earth sciences. Terra Nova 1(2):123–134

Allard D, D'Or D, Froidevaux R (2011) An efficient maximum entropy approach for categorical variable prediction. Eur J Soil Sci 62(3):381–393

Apanasovich TV, Genton MG (2010) Cross-covariance functions for multivariate random fields based on latent dimensions. Biometrika 97(1):15–30

Armstrong M, Galli A, Beucher H, Loc'h G, Renard D, Doligez B, . . . Geffroy F (2011) Plurigaussian simulations in geosciences. Springer Science & Business Media, New York

Burgess P, Wright V, Emery D (2001) Numerical forward modelling of peritidal carbonate parasequence development: implications for outcrop interpretation. Basin Res 13(1):1–16

Carle SF, Fogg GE (1996) Transition probability-based indicator geostatistics. Math Geol 28 (4):453–476

Catuneanu O, Galloway WE, Kendall CGSC, Miall AD, Posamentier HW, Strasser A, Tucker ME (2011) Sequence stratigraphy: methodology and nomenclature. Newslett Stratigr 44 (3):173–245

Chilès J-P, Delfiner P (2012) Geostatistics: modeling spatial uncertainty, vol 713. Wiley, Hoboken

D'Or D, Allard D, Biver P, Froidevaux R, Walgenwitz A (2008) Simulating categorical random fields using the multinomial regression approach. Paper presented at the Geostats 2008—proceedings of the eighth international geostatistics congress

Dubrule O (2016) Indicator variogram models – do we have much choice?. Manuscript submitted for publication

Egenhoff SO, Peterhänsel A, Bechstädt T, Zühlke R, Grötsch J (1999) Facies architecture of an isolated carbonate platform: tracing the cycles of the Latemar (Middle Triassic, northern Italy). Sedimentology 46(5):893–912

Fischer AG (1964) The Lofer cyclothems of the alpine Triassic. Princeton University, Princeton

Genz A (1992) Numerical computation of multivariate normal probabilities. J Comput Graph Stat 1(2):141–149

Genz A, Bretz F, Miwa T, Mi X, Leisch F, Scheipl F, Hothorn T (2009) mvtnorm: multivariate normal and t distributions. R package version 0.9-8. URL http://CRAN.R-project.org/package=mvtnorm

Gneiting T, Kleiber W, Schlather M (2012) Matérn cross-covariance functions for multivariate random fields. J Am Stat Assoc 105(491):1167–1177

Goldhammer R, Dunn P, Hardie L (1990) Depositional cycles, composite sea-level changes, cycle stacking patterns, and the hierarchy of stratigraphic forcing: examples from Alpine Triassic platform carbonates. Geol Soc Am Bull 102(5):535–562

Grotzinger JP (1986) Cyclicity and paleoenvironmental dynamics, Rocknest platform, northwest Canada. Geol Soc Am Bull 97(10):1208–1231

Kendall M, Stuart A, Ord J (1994) Vol. 1: Distribution theory. Arnold, London

Lantuéjoul C (2002) Geostatistical simulation: models and algorithms. Springer Science & Business Media, Berlin

Li B, Zhang H (2011) An approach to modeling asymmetric multivariate spatial covariance structures. J Multivar Anal 102(10):1445–1453

Masetti D, Neri C, Bosellini A (1991) Deep-water asymmetric cycles and progradation of carbonate platforms governed by high-frequency eustatic oscillations (Triassic of the Dolomites, Italy). Geology 19(4):336–339

Oliver DS (2003) Gaussian cosimulation: modelling of the cross-covariance. Math Geol 35 (6):681–698

Renard D, Bez N, Desassis N, Beucher H, Ors F, Laporte F (2015) RGeostats: the geostatistical package (Version 11.0.1). Retrieved from http://cg.ensmp.fr/rgeostats

Sena CM, John CM (2013) Impact of dynamic sedimentation on facies heterogeneities in Lower Cretaceous peritidal deposits of central east Oman. Sedimentology 60(5):1156–1183

Sheppard W (1899) On the application of the theory of error to cases of normal distribution and normal correlation. Philos Trans R Soc London Ser A Containing Pap Math Phys Charact 192:101–531

Strasser A (1988) Shallowing-upward sequences in Purbeckian peritidal carbonates (lowermost Cretaceous, Swiss and French Jura Mountains). Sedimentology 35(3):369–383

Tucker M (1985) Shallow-marine carbonate facies and facies models. Geol Soc London Spec Publ 18(1):147–169

Venables WN, Ripley BD (2002) Modern applied statistics with S, 4th edn. Springer, New York

Wackernagel H (2013) Multivariate geostatistics: an introduction with applications. Springer Science & Business Media, Berlin